

# Structural Insight into the Mechanism of Double-Stranded RNA Processing by Ribonuclease III

Jianhua Gan,<sup>1</sup> Joseph E. Tropea,<sup>1</sup> Brian P. Austin,<sup>1</sup> Donald L. Court,<sup>1</sup> David S. Waugh,<sup>1</sup> and Xinhua Ji<sup>1,\*</sup>

<sup>1</sup>Center for Cancer Research, National Cancer Institute, National Institutes of Health, Frederick, MD 21702, USA

\*Contact: [jix@ncifcrf.gov](mailto:jix@ncifcrf.gov)

DOI 10.1016/j.cell.2005.11.034

## SUMMARY

Members of the ribonuclease III (RNase III) family are double-stranded RNA (dsRNA) specific endoribonucleases characterized by a signature motif in their active centers and a two-base 3' overhang in their products. While Dicer, which produces small interfering RNAs, is currently the focus of intense interest, the structurally simpler bacterial RNase III serves as a paradigm for the entire family. Here, we present the crystal structure of an RNase III-product complex, the first catalytic complex observed for the family. A 7 residue linker within the protein facilitates induced fit in protein-RNA recognition. A pattern of protein-RNA interactions, defined by four RNA binding motifs in RNase III and three protein-interacting boxes in dsRNA, is responsible for substrate specificity, while conserved amino acid residues and divalent cations are responsible for scissile-bond cleavage. The structure reveals a wealth of information about the mechanism of RNA hydrolysis that can be extrapolated to other RNase III family members.

## INTRODUCTION

Ribonuclease III (RNase III) represents a highly conserved family of double-stranded RNA (dsRNA) specific endoribonucleases (Court, 1993; Filippov et al., 2000; Krainer, 1997; Nicholson, 1996, 1999; Robertson et al., 1968). It plays important roles in RNA processing (Robertson et al., 1968) and posttranscriptional gene-expression control (Court, 1993; Krainer, 1997; Wu et al., 2000). RNase III has gained added importance with the recent discovery of the role that Dicer plays in RNA interference, a broad class of

gene-silencing phenomena initiated by dsRNA (Bernstein et al., 2001; Carthew, 2001). The RNase III family can be divided into four classes with increasing molecular weight and complexity of the polypeptide chain, exemplified by bacterial RNase III, *Saccharomyces cerevisiae* Rnt1p, *Drosophila melanogaster* Drosha, and *Homo sapiens* Dicer, respectively (Blaszczak et al., 2004). The bacterial RNase III proteins, such as *Escherichia coli* RNase III (Ec-RNase III) and *Aquifex aeolicus* RNase III (Aa-RNase III), are composed of an endonuclease domain (endoND) followed by a dsRNA binding domain (dsRBD). In addition to an endoND and a dsRBD, Rnt1p has an N-terminal domain of ~200 amino acid residues (Lamontagne et al., 2001). Drosha has a large N-terminal extension of ~900 amino acid residues followed by two endoNDs and one dsRBD (Filippov et al., 2000). Finally, Dicer has two endoNDs, one dsRBD, and an even larger N-terminal extension of ~1500 amino acid residues that includes an RNA helicase domain and a PAZ (Piwi Argonaute Zwillie) domain (Bernstein et al., 2001). The sequence of the endoND is characterized by a stretch of conserved residues (<sub>37</sub>ERLEFLGD<sub>44</sub> in Aa-RNase III), which is known as the RNase III signature motif and makes up a large part of the active center.

Since its discovery in 1968 (Robertson et al., 1968), the homodimeric Ec-RNase III has become the most extensively studied member of the family. It can affect gene expression in either of two ways: as a processing enzyme or as a binding protein. As a processing enzyme, RNase III cleaves both natural and synthetic dsRNA into small duplex products averaging 10–18 base pairs in length (Court, 1993; Dunn, 1982; Robertson, 1982; Robertson and Dunn, 1975). As a binding protein, RNase III binds and stabilizes certain RNAs, thus suppressing the expression of certain genes (Calin-Jageman and Nicholson, 2003; Court, 1993; Dasgupta et al., 1998; Guarneros, 1988; Oppenheim et al., 1993). In vitro, both Dicer and Ec-RNase III can be used to cleave long dsRNA, producing small interfering RNA cocktails that are effective mediators of gene silencing (Yang et al., 2002).

Previously, we reported three endoND structures of Aa-RNase III with and without bound metal ions, which reveal a symmetric endoND dimer with a ball-and-socket junction at each end of the subunit interface, a catalytic valley that can accommodate a dsRNA substrate, and a cluster of six acidic side chains (E37, E40, D44, D107, and E110 from

one subunit and E64 from the partner subunit, among which E37, E40, and D44 are located in the signature motif located at each end of the valley (Blaszczyk et al., 2001). On the basis of the structural and biochemical data, catalytic models were proposed before the structure of a catalytic complex became available. Among the six acidic side chains, E110 was proven to be essential for catalysis (Blaszczyk et al., 2004; Dasgupta et al., 1998; Inada et al., 1989; Li and Nicholson, 1996). In addition, our in vivo data suggested that E37, D44, and E64 are also essential, which led to our model of compound active centers, each containing two different RNA cleavage sites, D44/E110 and E37/E64 (Blaszczyk et al., 2001). Further in vitro data supported the essential role of D44 but not the roles of E37 and E64 (Lee et al., 2004; Zhang et al., 2004), which led to the single-processing-center model, containing two identical RNA cleavage sites, D44/E110 (Zhang et al., 2004). We were puzzled about the functional roles of E37 and E64 because the in vitro data also indicated their involvement in catalysis although they are not essential (Sun et al., 2004; Zhang et al., 2004). To establish the functional roles of these two side chains and to understand the mechanism of dsRNA processing by RNase III enzymes, it is necessary to gain structural insights on the details of catalytic complex. After determining five crystal structures of Aa-RNase III•dsRNA in various noncatalytic forms of the complex (Blaszczyk et al., 2004; Gan et al., 2005), we succeeded in determining the crystal structure of a catalytic complex. Here, we present the structure of an RNase III-product complex and describe in detail the protein-RNA interactions that are responsible for the recognition and binding of dsRNA, substrate specificity, and scissile-bond selection.

## RESULTS AND DISCUSSION

Although the *E. coli* enzyme is the most extensively studied member of the RNase III family, structural information for RNase III has thus far been restricted to enzymes from other bacteria, especially *A. aeolicus* (Blaszczyk et al., 2001, 2004; Gan et al., 2005). Accordingly, in the following sections, we will use the amino acid residue numbers of Aa-RNase III unless otherwise stated. Residue numbers for Ec-RNase III can be found in Blaszczyk et al. (2004), and those for Dicer can be found in Zhang et al. (2004).

### Aa-D44N, a Mutant RNase III with Greatly Reduced Activity

In our effort to crystallize a catalytic complex of RNase III, we focused on two mutant proteins, Aa-D44N and Aa-E110Q, and succeeded in determining the crystal structure of Aa-D44N with dsRNA bound in its catalytic valley.

Residues D44 (of the signature motif) and E110, located in the active center of RNase III, are strictly conserved in all members of the family (Blaszczyk et al., 2001). It was found that the D44N mutant (Sun et al., 2004) had greatly reduced RNA cleavage activities although its RNA binding affinity was comparable to that of the wild-type enzyme; only after extended reaction times at high enzyme concentrations was

a low level of catalytic activity observed (Sun et al., 2004). Similar to the D44 mutant, the E110Q mutant had negligible RNA cleavage activity but retained its RNA binding affinity; however, E110Q did not show any catalytic activity over extended reaction time and at high protein concentrations (Sun and Nicholson, 2001).

### RNA 5, a Designed Substrate

In our previously reported RNase III•dsRNA structures (Blaszczyk et al., 2004; Gan et al., 2005), four RNAs were used: RNA 1 (5'-GGCGCGCGCC-3'), RNA 2 (5'-CGAACUUCGCG-3'), RNA 3 (5'-AAAUUAUUAUUU-3'), and RNA 4 (5'-CGCGAAUUCGCG-3'). All four RNAs form self-complementary duplexes. In the crystal lattice, each of these RNA duplexes stacks end to end as a pseudocontinuous helix. To avoid this extended stacking, we designed a stem-loop RNA molecule (RNA 5, Figure 1A) containing a four-base loop (GCAA) that can prevent base stacking from that end. RNA 5 was derived in part from mini-R1.1[WC] RNA (Nicholson, 1999), which was in turn derived from R1.1[WC] RNA, a canonical substrate of Ec-RNase III (Zhang and Nicholson, 1997).

### RNA 6, a Product of Aa-D44N-Catalyzed RNA 5 Hydrolysis

We expected to crystallize a catalytic complex in the form of either Aa-D44N•RNA 5 or Aa-E110Q•RNA 5, but what we obtained in the crystal was Aa-D44N in complex with an RNA cleavage product of RNA 5, which we refer to as RNA 6 (Figures 1B and 1C). One must bear in mind that the D44N mutant of Ec-RNase III retains a low level of RNA cleavage activity at high enzyme concentration over an extended period of time (Sun et al., 2004) and that the Aa-D44N-RNA 5 mixture was heated at 75°C for 30 min before the crystallization experiments were set up, which may be within the temperature range of optimum activity for thermophilic *A. aeolicus* enzymes. Crystals appeared 3 months later and reached the dimensions of 0.10 × 0.10 × 0.02 mm after 1 more month. The protein-product complex contains one Aa-D44N dimer and two RNA 6 molecules, in which the two RNA 6 molecules stack as an A form pseudocontinuous duplex via complementary overlapping of two-base 3' overhangs. How the complex was formed is not clear, and it could be formed through several different pathways. The two RNA 6 molecules in the complex can also represent the products from double-stranded cleavage of a longer substrate. The overall structure of Aa-D44N•RNA 6 is depicted in Figure 2.

### Overall Structure, a Symmetric Dicing Machine

The structure of Aa-D44N•RNA 6 was determined at 2.05 Å resolution. The complex is composed of 2 Aa-D44N subunits (each containing 218 amino acid residues), 2 RNA 6 molecules (each containing 28 nucleotide residues), 2 Mg<sup>2+</sup> ions, and 298 water oxygen atoms. The two N-terminal amino acid residues and the C-terminal residue of the polypeptide chain were not observed. The entire structure of the complex is highly symmetric.

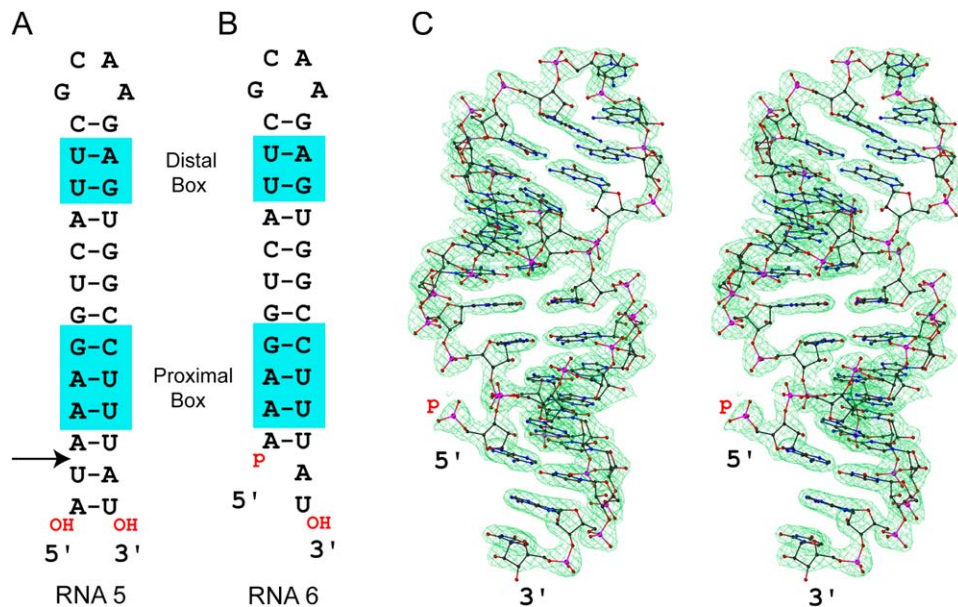


**Figure 1. Substrate (RNA 5) and a Product (RNA 6) of Aa-RNase III (D44N)**

(A) Sequence and structure of RNA 5. Scissile bond is indicated with an arrow. Cyan rectangles indicate the distal box and proximal box (Zhang and Nicholson, 1997).

(B) Sequence and structure of RNA 6, one of the two products of Aa-D44N-catalyzed RNA 5 cleavage. The other product is a dinucleotide (5'-AU-3').

(C) Stereoview showing the composite annealed omit map ( $2F_o - F_c$ , contoured at 1.0  $\sigma$  level) of RNA 6. The RNA is illustrated as stick models in atomic color scheme (carbon in black, nitrogen in blue, oxygen in red, and phosphorus in pink), and the electron density map is shown as a green net.

The view in Figure 2A is along the 2-fold axis by which the two Aa-D44N subunits and the two RNA 6 molecules are related. In each of the two cleavage sites, the 5' phosphate group of the RNA 6 molecule is located in proximity to the  $Mg^{2+}$  ion. The root-mean-square deviation (rmsd) for all C $\alpha$  atoms between the two polypeptide chains that comprise the homodimer (a total of 218 target pairs) is 0.30 Å, and the rmsd for all atoms between the two RNA 6 molecules (594 target pairs) is 0.50 Å.

The view in Figure 2B is along the long axis of the RNA pseudoduplex, showing the tight fit of the RNA to the protein. The entire structure resembles a clamp that cradles the dsRNA in the midst of the four domains. The total buried surface area between the protein and the RNA is 5220 Å<sup>2</sup>, including 1880 Å<sup>2</sup> between the RNA and the two endoNDs and 3340 Å<sup>2</sup> between the RNA and the two dsRBDs, underscoring the dominant role of the dsRBDs in dsRNA binding. Dicer has two endoNDs and one dsRBD, with the two endoNDs forming an intramolecular dimer (Zhang et al., 2004). Compared to dimeric bacterial RNase III, one dsRBD is not present in Dicer, suggesting that a single dsRBD may be sufficient for RNase III function. Studies on a number of dsRBD-containing proteins showed that a single dsRBD is indeed sufficient to provide the protein with a clear specificity for target selection (Chang and Ramos, 2005).

#### Structural Basis for Induced Fit

Recently, the full-length RNase III from *Mycobacterium tuberculosis* was crystallized and the structure determined at

2.1 Å resolution, but the position of dsRBD is totally disordered (Akey and Berger, 2005). In the five Aa-RNase III-dsRNA structures we reported previously, the relative orientations between the endoNDs and the dsRBDs vary dramatically (Blaszczuk et al., 2004; Gan et al., 2005). Comparison between the structure of Aa-D44N•RNA 6 (Figure 3A) with the structure of RNA-free *Thermotoga maritima* RNase III (Tm-RNase III, Protein Data Bank [PDB] ID code 1O0W) (Figure 3B) indicates a dramatic rotation and shift of the dsRBD due to RNA binding. The structural basis for the induced fit of RNase III is provided by the presence of a linker (<sub>145</sub>EGRVKKD<sub>151</sub>) between the endoND and the dsRBD (Figure 3C). Because both the endoND and the dsRBD are relatively rigid, the flexibility of the linker is responsible for major conformational changes within the molecule. Before any structural information was available, genetic evidence indicated that the linker segment was important. Residue Q153 of Ec-RNase III is located in the middle of the linker (Figure 3C). The Q153P substitution in Ec-RNase III abolished RNA cleavage activity but retained dsRNA binding activity (Inada and Nakamura, 1995). This residue is not conserved, and in Aa-RNase III, the analogous residue is K149 (Figure 3C). In the crystal structure of Aa-D44N•RNA 6, the side chain of K149 is disordered (Figure 3D). Perhaps the significance of the Ec-RNase III Q153P mutation resides in the mutational change to a Pro residue in the middle of the linker, which may reduce the flexibility of the segment. Thus, reorientation of the dsRBD•dsRNA structure may be inhibited in the mutant. On the other hand, it was shown that

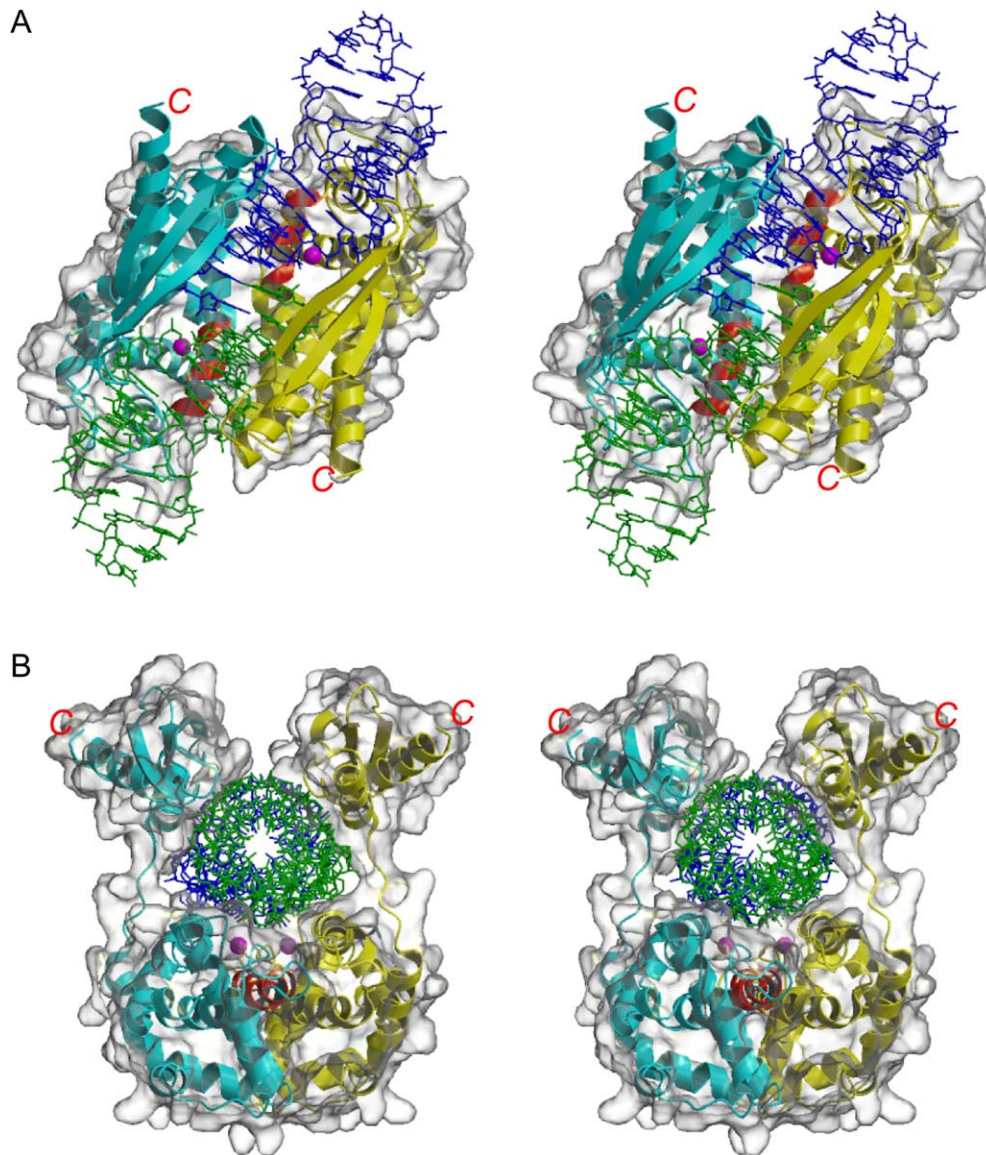


**Figure 2. The Overall Structure of the Aa-D44N•RNA 6 Complex**

(A) Stereoview of the symmetric structure of the product complex Aa-D44N•RNA 6. The two endoNDs are outlined with transparent surfaces. The protein is illustrated as ribbon diagrams (helices as spirals,  $\beta$  strands as arrows, and loops as pipes) with the two subunits colored in cyan and yellow. The signature motif is highlighted in red, the  $Mg^{2+}$  ions in purple, and the two RNA 6 molecules in blue and green.

(B) Stereoview of Aa-D44N•RNA 6 along the long axis of the RNA pseudoduplex. In this view, the dsRBD is also outlined with transparent surfaces.

extension of the linker from 9 to 20 amino acids in Ec-RNase III does not affect cleavage-site selection (Conrad et al., 2001).

Among the 7 residues in the linker, the last one is a highly conserved aspartate (Figure 3C). It was found that the Ec-RNase III (D155E) mutant did not bind dsRNA (Inada and Nakamura, 1995), suggesting that a very precise positioning of the carboxylic-acid functional group is important for RNA binding. In the current structure, the distance between the aspartate side chain and the bound RNA is  $\sim 3.2$  Å. Therefore, the larger glutamate side chain at position 155 likely

creates steric hindrance against the recognition and binding of dsRNA by the dsRBD. We have observed, in all of our Aa-RNase III-dsRNA structures thus far determined, that the side chain of D151 forms a hydrogen bond with the side chain of highly conserved residue T154, and the T154 side chain forms a hydrogen bond with an  $O2'$  hydroxyl (Figure 3E). It appears that T154 is required for RNA recognition and that D151 is responsible for keeping the Thr side chain in the proper orientation. In addition, the interaction between D151 and T154 also forms the N-terminal cap of the first  $\alpha$  helix of the dsRBD and therefore stabilizes this helix. As

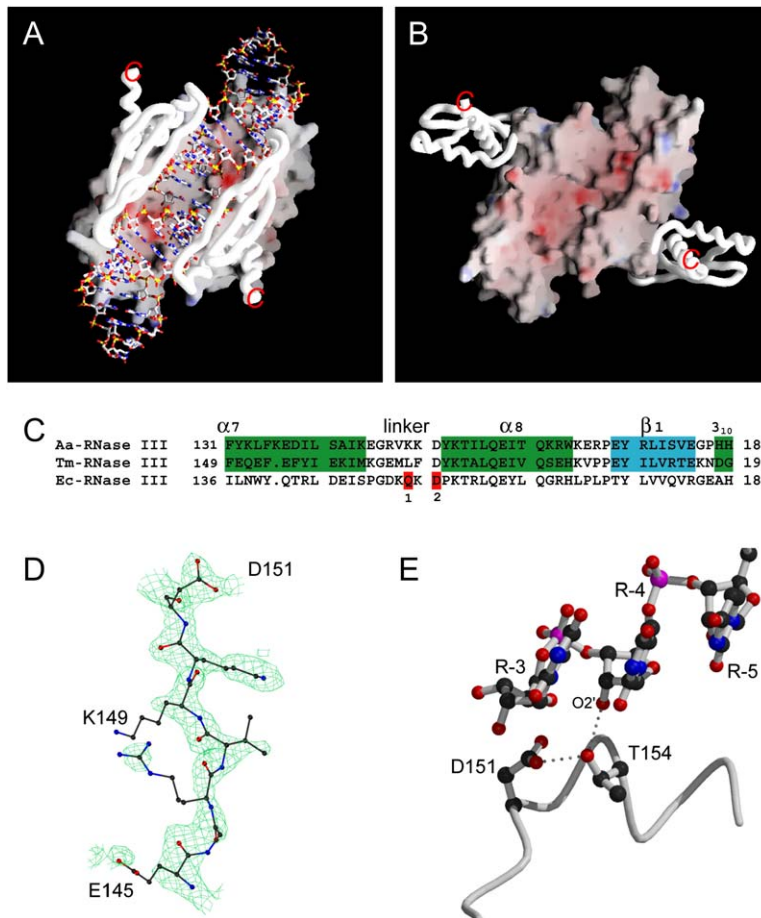


**Figure 3. The Flexible Linker and Induced Fit during dsRNA Binding**

(A and B) Schematic illustration of the Aa-D44N•RNA 6 structure (A) showing a dramatic rotation and shift of dsRBD with respect to the endoND when compared to the RNA-free Tm-RNase III structure (PDB ID code 100W) (B). The endoNDs are illustrated as molecular surface with positive and negative potentials indicated by blue and red colors, respectively. The dsRBDs are shown as C $\alpha$  backbone worms in white.

(C) Amino acid sequences of Aa-RNase III, Tm-RNase III, and Ec-RNase III in the linker and nearby regions. Color shading indicates secondary-structure elements (helices in green,  $\beta$  strands in cyan) and two single-mutation sites (in red) in the linker region: 1, *mc10* (Ec-Q153P) and 2, *mc7* (Ec-D155E) (Inada and Nakamura, 1995).

(D) The structure of the 7 residue linker outlined with annealed omit map ( $2F_o - F_c$  contoured at  $1.0 \sigma$ ) in the Aa-D44N•RNA 6 structure.

(E) Residue D151 forms a hydrogen bond with T154 that in turn forms a hydrogen bond to an O2' hydroxyl of RNA. Amino acid residues are shown as ball-and-stick models, the electron density map as a green net, and the C $\alpha$  trace as a gray worm.

an RNA binding motif, the first helix of the dsRBD plays an important role in the recognition and binding of dsRNA.

### The Four RNA Binding Motifs in RNase III

The binding of dsRNA by RNase III in all observed forms of protein-RNA complex is dominated by the dsRBD. However, both the dsRBD and the endoND contribute to substrate specificity. The Aa-D44N•RNA 6 structure provides the opportunity to identify RNA binding motifs (RBMs; Figure 4A) in RNase III and protein-interacting boxes in the dsRNA (Figure 5A), which define the protein-RNA interactions in detail.

RBM 1 is the first  $\alpha$  helix of the dsRBD (Figure 3C), in which residues T154, Q161, Q157, and E158 each form a hydrogen bond with an O2' hydroxyl of RNA (Figure 4B). There are three more hydrogen bonds between amino acid side chains and the O2' hydroxyls of RNA, one for each of the remaining RBMs. Therefore, although all four RBMs are important, RBM 1 appears to be the most important for the recognition and binding of dsRNA. In the catalytic complex, RBM 1 interacts with the proximal box of RNA (Zhang and Nicholson, 1997), which is only 1 base pair from the scissile bond (Figure 5A). Therefore, RBM 1 may also play a role in organizing the cleavage-site structure.

RBM 2 is the loop between  $\beta$  strands 1 and 2 of the dsRBD (residues 177–182; Blaszczyk et al., 2001). It fits into the minor groove of bound dsRNA but flips and points in the opposite direction when no RNA is bound (Figure 4C). RBM 2 interacts with two base pairs of RNA between the proximal box and distal box (Zhang and Nicholson, 1997). One hydrogen bond is formed between an O2' hydroxyl and the side chain of RBM 2 residue H180. We refer to these two base pairs as the “middle box” (Figure 5A).

RBM 3 is the N-terminal portion of  $\alpha$  helix 4 (residues 64–68; Blaszczyk et al., 2001). Residues E64 and S68 are involved in dsRNA binding. Without bound substrate, a hydrogen bond is formed between the two side chains (Blaszczyk et al., 2001). Upon RNA binding, S68 forms a hydrogen bond with the O2' hydroxyl of R 0, the nucleotide residue in the cleavage site, and the side chain of E64 protrudes into the major groove and forms a hydrogen bond with a phosphate oxygen of nucleotide residue R+1 (Figure 4D). Upon RNA binding, no noticeable conformational change is observed for S68, whereas the side chain of E64 undergoes significant changes. The interactions between RBM 3 and nucleotide residues R 0 and R+1 determine the scissile bond and may also help optimize the cleavage-site structure.

RBM 4 is the loop between  $\alpha$  helices 5 and 6 in the endoND (residues 92–102; Blaszczyk et al., 2001). Projecting

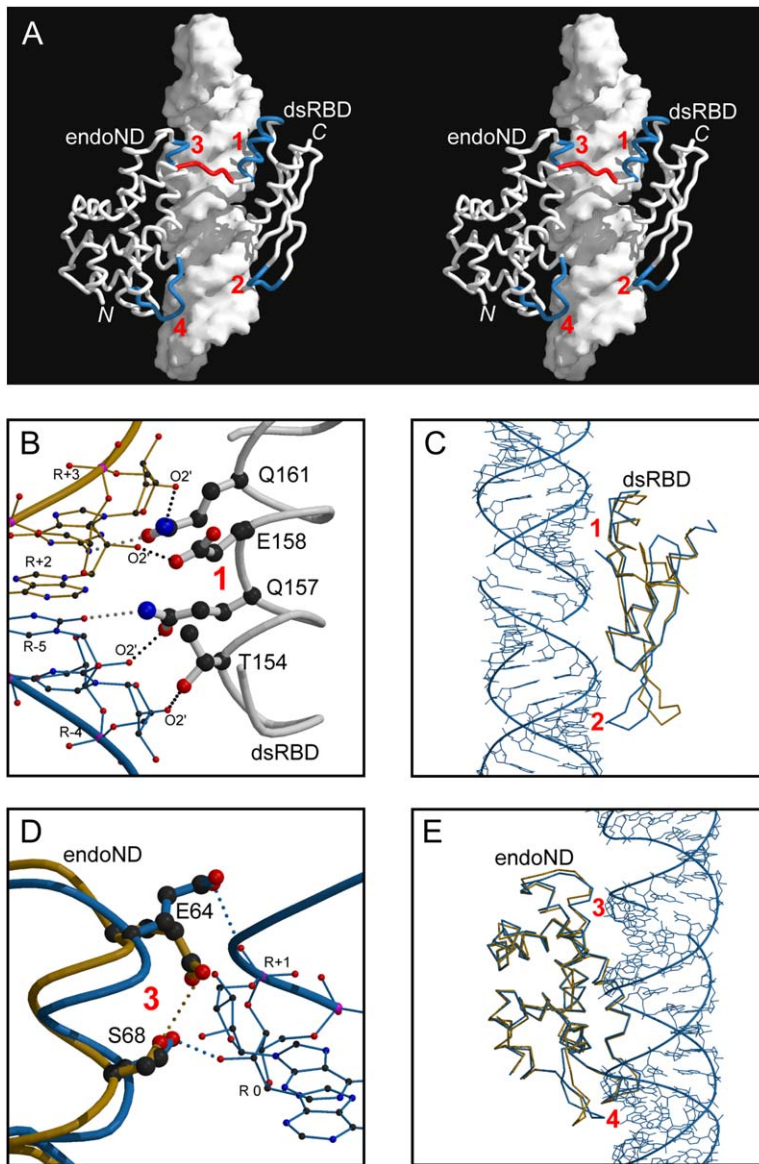


**Figure 4. RNA Binding Motifs and Substrate Specificity of RNase III**

(A) Stereoview showing the location of the four RNA binding motifs (RBMs). Only one subunit of RNase III is shown for clarity. The dsRNA is illustrated as a molecular surface model and the protein as a backbone worm with the linker between the endoND and dsRBD and the four RBMs highlighted in red and blue, respectively.

(B) Dotted lines indicate hydrogen bonds between RBM 1 and the O2' hydroxyls (in black) or between RBM 1 and the bases (in gray). Residues are represented by ball-and-stick models in atomic color scheme (carbon in black, nitrogen in blue, oxygen in red, and phosphorus in purple). Also shown are the backbones of  $\alpha$ 8 and the dsRNA.

(C)  $\alpha$ -based alignment between a dsRBD in the Aa-D44N•RNA 6 complex (in blue) and a dsRBD in RNA-free Tm-RNase III (in orange; PDB accession code 1OOW).

(D)  $\alpha$ -based alignment between an RBM 3 in the Aa-D44N•RNA 6 complex (in blue) and an RBM 3 in the Aa-endoND•Mg<sup>2+</sup> structure (in orange; Blaszczyk et al., 2004).

(E)  $\alpha$ -based alignment between one endoND in the Aa-D44N•RNA 6 complex (in blue) and one endoND in the noncatalytic complex Aa-E110K•RNA 1 (in orange; Blaszczyk et al., 2004).

into the minor groove of dsRNA (Figure 4E), RBM 4 interacts with the distal box (Figure 5A). Between an O2' hydroxyl of the RNA and the side chain of R97, a hydrogen bond is formed. The distance between RBMs 3 and 4 is fixed in the endoND dimer. Thus, RBM 4 binding could also help determine where RBM 3 binds and could play a role in selecting the scissile bond.

The four RBMs collectively recognize and bind a dsRNA substrate by forming seven hydrogen bonds with O2' hydroxyls and projecting two loops (RBMs 2 and 4) into the minor groove. Therefore, each RNase III dimer uses 14 hydrogen bonds to recognize the O2' hydroxyls and 4 loops to recognize the minor groove of a dsRNA substrate. In addition, 49 hydrogen bonds and 11 salt bridges are formed directly between the protein and the RNA, and 23 water molecules are found to bridge the interactions between amino

acid and nucleotide residues with 72 hydrogen bonds. Approximately two-thirds of these interactions are between the dsRBDs and the RNA, in agreement with the results of buried surface analysis.

A plausible pathway for the formation of a substrate complex may include three steps: (1) One dsRBD binds to a dsRNA via RBMs 1 and 2. (2) This dsRBD brings the bound RNA in proximity to the endoNDs (or the endoNDs approach the bound RNA) for substrate recognition. (3) Once the dsRNA is recognized by RBMs 3 and 4, the second dsRBD binds to and locks the substrate in position. Although the assembly of a productive complex does not necessarily occur by this pathway, the protein-RNA interactions observed in the complex indicate that RBMs 1 and 2 play dominant roles in the recognition and binding of dsRNA, whereas RBMs 3 and 4 are dominant in substrate specificity

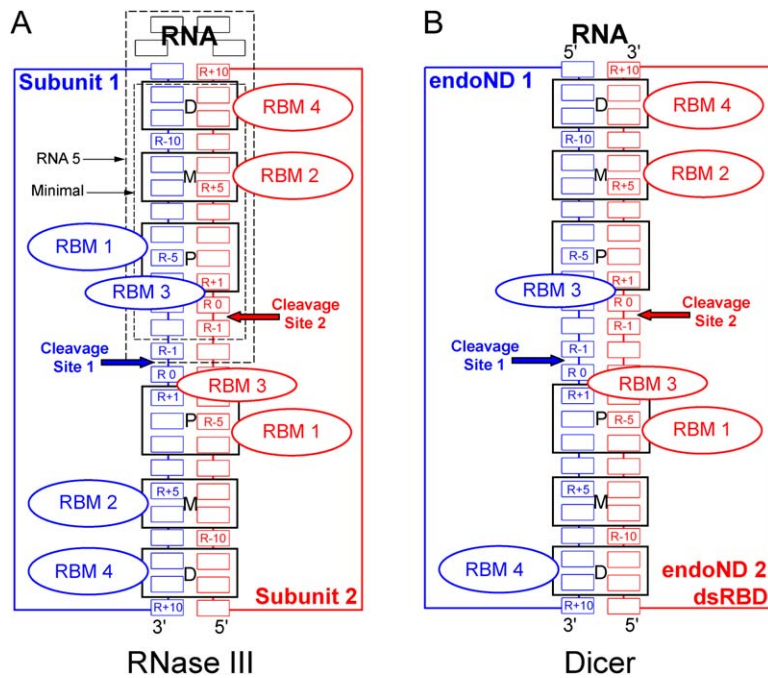


**Figure 5. Schematic Representation of RNase III-dsRNA Interactions**

(A) The RNase III-dsRNA interactions observed in the structure of Aa-D44N•RNA 6 are schematically illustrated. The dimeric protein is shown as two rectangles and is labeled as “Subunit 1” and “Subunit 2,” and the four RBMs are shown as ellipsoids. The substrate is represented by a stem-loop dsRNA with a 24 base pair double-stranded region. The scissile bonds are indicated with arrows, and the protein-interacting boxes in the dsRNA (proximal, middle, and distal boxes) are outlined with rectangles and indicated with one-letter abbreviations for clarity. The nucleotide residues in the cleavage sites are numbered “R 0,” and the rest are numbered according to the polarity of the RNA strand. Subunit 1 of RNase III and associated RNA strand are outlined in blue; subunit 2 and associated RNA substrate are indicated in red. RNA 5 and minimal dsRNA substrate are indicated with dashed lines. RBMs 1, 2, and 4 interact with the proximal, middle, and distal box of the dsRNA, respectively, whereas RBM 3 interacts with nucleotide residues R 0 and R+1 of a single RNA strand.

(B) Dicer-dsRNA interactions. In this panel, the left rectangle represents endoND 1 (in blue) and the right rectangle represents endoND 2 and dsRBD (in red) of Dicer.

and scissile-bond selection. Dicer has two endoNDs, which dimerize intramolecularly (Zhang et al., 2004), but only one dsRBD, which appears to be sufficient for the recognition and binding of dsRNA (Figure 5B). Note that RBMs 1 and 2 do not discriminate against nonsubstrate dsRNA; it was shown that Rnt1p binds to an RNA that has a 5 base pair stem of only one helical turn (Lamontagne et al., 2003). It is RBMs 3 and 4 that discriminate against nonsubstrate dsRNA. A truncated form of Ec-RNase III without dsRBD (i.e., without RBMs 1 and 2) was shown to accurately cleave certain processing substrates in vitro (Sun et al., 2001); in *Mycoplasma genitalium* and *Mycoplasma pneumoniae*, the RNase III does not have a dsRBD (Tian et al., 2004). For longer dsRNA substrates of at least 22 base pairs, RBMs 3 and 4 in both subunits function together, recognizing the substrate and determining the scissile bonds on both strands of the substrate (Figure 5A). For shorter dsRNAs with one scissile bond, such as RNA 5, substrate recognition and scissile-bond selection can be achieved by a mixed set of RBMs 3 and 4, i.e., RBM 3 from one subunit and RBM 4 from the partner subunit (Figure 5A).

An Aa-RNase III dimer has two sets of four RBMs. For the cleavage of shorter substrates such as RNA 5, a mixed set of four RBMs is involved, of which RBMs 1 and 3 are from one subunit while RBMs 2 and 4 are from the partner subunit (Figure 5A). Although the amino acid sequences of the RBMs may not be conserved, we believe that the pattern of interactions between the four RBMs in RNase III and the three boxes in the dsRNA is conserved. For example, the hydrogen bonds from RBMs 1 and 2 to the O2' hydroxyl groups of dsRNA were first identified in the crystal structure of the

second dsRBD of *Xenopus laevis* RNA binding protein A in complex with dsRNA (Ryter and Schultz, 1998) and were later also observed for several other dsRNA binding proteins (Chang and Ramos, 2005; Tian et al., 2004).

Although RNase III is able to bind a dsRNA consisting of only one helical turn, the normal substrate length is two helical turns of A form dsRNA (Conrad and Rauhut, 2002; Court, 1993). RNA 5, the stem-loop substrate containing a 13 base pair stem, is cleaved by Aa-D44N two bases from its 5' end (Figures 1A and 1B and Figure 5A). It was also shown that Rnt1p is able to cleave one base from the 5' end of a substrate (Lamontagne et al., 2003). Assuming that bacterial RNases III can do the same, their smallest dsRNA substrate should contain 11 base pairs to interact with a mixed set of RBM 3 and RBM 4 for substrate recognition and scissile-bond selection (Figure 5A).

### The Role of Dimerization in RNase III Function

The catalytic valley in the RNase III dimer is approximately 50 Å long and 20 Å wide. In the catalytic valley are located two clusters of six acidic side chains (E37, E40, D44, D107, and E110 from one subunit and E64 from the partner subunit, among which E37, E40, and D44 are signature motif residues). Each cluster coordinates to a metal ion, and the distance between the two metal ions is 22.4 Å (Blaszczuk et al., 2001). Residue E110 was proven to be essential for catalysis (Blaszczuk et al., 2004; Dasgupta et al., 1998; Inada et al., 1989; Li and Nicholson, 1996). Our in vivo data suggested that E37, D44, and E64 are also essential (Blaszczuk et al., 2001). Further in vitro data supported the essential role of D44 but not the roles of E37 and E64 (Lee

et al., 2004; Zhang et al., 2004). Lee and coworkers found that mutation of these two residues in the first endoND of *Drosophila* Dicer does not inactivate the enzyme (Lee et al., 2004), while Zhang and coworkers discovered that the single Glu-to-Ala mutation at each of the two positions in Ec-RNase III or the first endoND of human Dicer produces a protein that has catalytic activity comparable to the wild-type but increased  $K_M$  values for the substrate (Zhang et al., 2004). Recently, Sun and coworkers found that the single Glu-to-Ala mutants at these positions in Ec-RNase III exhibit  $Mg^{2+}$ -dependent dsRNA cleavage activities: At the physiological level (1 mM  $Mg^{2+}$ ), the two single mutants exhibit catalytic activities that are about 18% that of the wild-type, whereas with 10 mM  $Mg^{2+}$ , both mutants show approximately 80% catalytic activity (Sun et al., 2004). The functional roles of these two side chains remained puzzling until we determined the present structure. On the basis of our new structural data, we conclude that E37 is involved in protein dimerization only and that E64, as an RBM 3 residue, is involved in substrate recognition and scissile-bond selection.

The crystal structure of the product complex indicates that a single RNA cleavage event occurs on each strand of the RNA within each cleavage site (Figure 2A and Figure 5). For each cleavage event, residues S68 and E64 (RBM 3) from one subunit select the scissile bond (Figure 5A), and the hydrolysis of the scissile bond is carried out by conserved residues E40, D44, D107, and E110 from the partner subunit. Hence, dimerization of the endoNDs is essential for RNase III function. Also, dimerization makes it possible for the enzyme to recognize shorter substrates with a mixed set of four RBMs (Figure 5A).

### The Roles of Conserved Amino Acid Residues and Cofactors in the Cleavage Site

The RNase III-catalyzed dsRNA cleavage is  $Mg^{2+}$  ion dependent and probably proceeds in a single step via an  $S_N2$  (bimolecular nucleophilic substitution) type mechanism (Campbell et al., 2002; Dunn, 1982; Li and Nicholson, 1996; Robertson et al., 1968; Sun and Nicholson, 2001). The Aa-D44N•RNA 6 structure reveals that each RNA cleavage site is composed of amino acid residues E40, D44, D107, and E110; nucleotide residues R-1, R 0, and R+1; the  $Mg^{2+}$  ion; and three water molecules (Figure 6A). The  $Mg^{2+}$  ion coordinates with three acidic side chains (E40, D107, and E110) and the three water molecules (1, 2, and 3), assuming the geometry of an octahedron. In addition to interacting with the metal ion, E110 is also hydrogen bonded to water 2 that, together with water 1, interacts with the 5' phosphate of RNA 6 (Figure 6A). The coordination of  $Mg^{2+}$  in the product complex is slightly different from the one we previously observed in the RNA-free structures (Blaszczuk et al., 2001, 2004). All components of the  $Mg^{2+}$  coordination adjust slightly upon RNA binding. Water molecules 2 and 3 undergo the most significant adjustment, such that the plane defined by  $Mg^{2+}$  and these two water molecules appears to swing around the  $Mg^{2+}$  ion back and forth, in concert with the catalytic cycle, by  $\sim 40^\circ$  between the RNA-free and

RNA bound states (Figure 6B). Comparatively, the  $Mg^{2+}$  octahedron in the product complex is more distorted. Water molecule 2 always bridges the interaction between the metal ion and the D44 side chain, whereas water 3 is hydrogen bonded to the E110 side chain only in the RNA-free state (Figure 6B). Least affected upon RNA binding are the side chains of E40 and D107; neither is located in proximity to the scissile bond, in agreement with the previously proposed roles of E40 and D107 in metal binding (Sun et al., 2004). However, there is a stringent functional requirement for both the charge and size of the D44 and E110 side chains, which, together with their locations and their relationship with other components of the cleavage site, indicates the involvement of a second metal ion in the mechanism of RNase III catalysis. The structural data on functionally related enzymes, especially RNase H, suggests a position for the second metal ion.

RNase III enzymes belong to a superfamily of polynucleotidyl transferases that includes RNases, DNases, and transposases. Two-metal-ion catalysis was established for both Tn5 transposase (Davies et al., 2000; Steiniger-White et al., 2004) and RNase H (Nowotny et al., 2005) and was suggested for RNase III on the basis of biochemical data (Sun et al., 2005). Tn5 is specific for DNAs, and no water is involved in catalysis; RNase H is specific for RNA-DNA heteroduplexes, and two water molecules are involved in catalysis (Nowotny et al., 2005). Although RNase H is specific for RNA/DNA hybrid while RNase III is specific for dsRNA, the catalytic events for the two enzymes are the same (i.e., metal-dependent and sequence-nonspecific hydrolysis of an RNA phosphodiester bond). Therefore, the cleavage site of RNase III should resemble that of RNase H (Figure 7).

In the cleavage site of RNase H, four conserved acidic side chains (D71, E109, D132, and D192) coordinate with two  $Mg^{2+}$  ions, designated A and B (Nowotny et al., 2005). Metal ion A is six-coordinated with D71; D192; the pro- $S_p$  oxygen of the scissile-bond phosphate; and water molecules 1, 2, and 3, whereas metal B is five-coordinated with D132, D71, E109, O3' hydroxyl of the scissile bond, and the pro- $S_p$  oxygen of the scissile-bond phosphate. Metal A-coordinated water 3 is also hydrogen bonded to the carboxylate group of D132 (Figure 7). The coordination octahedron of the  $Mg^{2+}$  ion in RNase III can be aligned with that of metal A in RNase H such that residues E110 and D107 in RNase III superimpose with residues D71 and D192 in RNase H, respectively, and that two of the three water molecules, 1 and 3, superimpose (Figure 7). This alignment reveals two major differences between the two cleavage sites. First, although the two sites share the Asp-water-metal interaction, the spatial arrangement of the Asp-water-metal structure is different, one being an approximate mirror image of the other. Second, metal B in RNase H coordinates with one more acidic side chain (E109), whereas it is metal A in RNase III that coordinates with an extra acidic side chain (E40). This comparison also suggests that a conformational change takes place in the RNA during catalysis. There is a difference of  $\sim 3.0 \text{ \AA}$  in the position of the scissile-bond region between the substrate in the RNase H structure and the product in the

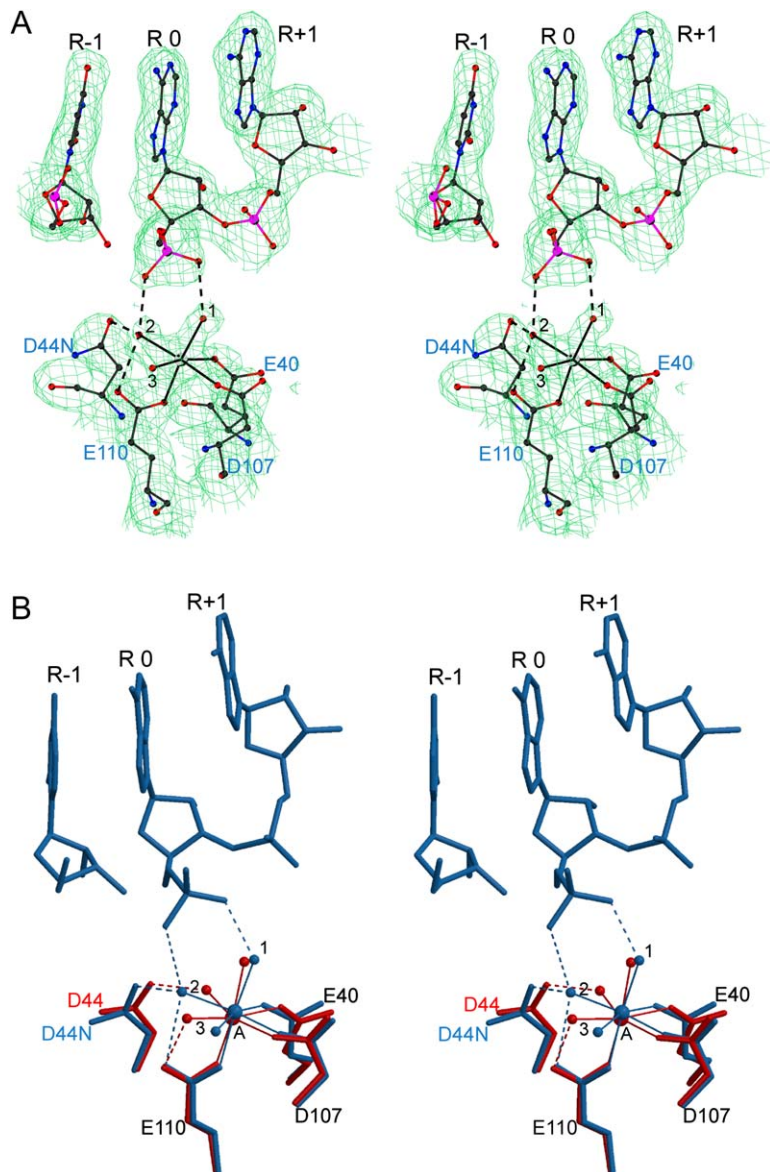


**Figure 6. Cleavage-Site Structure of RNase III with and without Bound RNA**

(A) Stereoview showing the cleavage site observed in the Aa-D44N•RNA 6 structure. Residues are shown as ball-and-stick models in atomic color scheme (carbon in black, nitrogen in blue, oxygen in red, phosphorus in purple, and magnesium in gray) outlined with annealed omit map in green ( $2F_o - F_c$  contoured at  $1.0 \sigma$ ). (B) Stereoview showing the superposition of the cleavage site in Aa-D44N•RNA 6 (in blue) and in Aa-endoND•Mg<sup>2+</sup> (in red; PDB ID code 1RC5; Błaszczyk et al., 2004). The coordination bonds are shown as solid lines and hydrogen bonds as dashed lines.

RNase III structure, which is likely to be the consequence of the presence or absence of the second metal ion (Figure 7). Accordingly, the product of RNase H should assume the product position observed in the RNase III structure when metal B is released, and the substrate of RNase III should adopt the substrate position seen in the RNase H structure if a second metal ion is indeed involved. The structures of both the RNase III-substrate complex and the RNase H-product complex remain to be determined.

### Conclusions

RNA 5, a 30 base stem-loop RNA of the sequence 5'-AU AAAGGUCAUUCGCAAGAGUGGCCUUAU-3', is cleaved by Aa-RNase III (D44N). The products of the reaction include a dinucleotide 5'-AU-3' and a 28 base stem-loop RNA with a two-base 3' overhang (RNA 6). Two RNA 6 molecules

and a dimeric Aa-D44N molecule form a product complex, which represents the first catalytic complex of RNase III with dsRNA. Induced fit, facilitated by a flexible linker between the endoND and the dsRBD, occurs in protein-RNA recognition. The overall structure of the complex is highly symmetric, with the protein-RNA interactions mediated by four RNA binding motifs (RBMs) in RNase III and three protein-interacting boxes in dsRNA. RNase III binds to both substrate and nonsubstrate dsRNAs. While RBMs 1 and 2 in the dsRBD are responsible for dsRNA recognition and binding, RBMs 3 and 4 in the endoND are responsible for substrate recognition and scissile-bond selection. Dimerization of endoNDs is essential for RNase III function in that residues from one subunit (RBM 3 residues) are involved in the selection of the scissile bond, while those from the partner subunit (strictly conserved residues) are involved in the cleavage

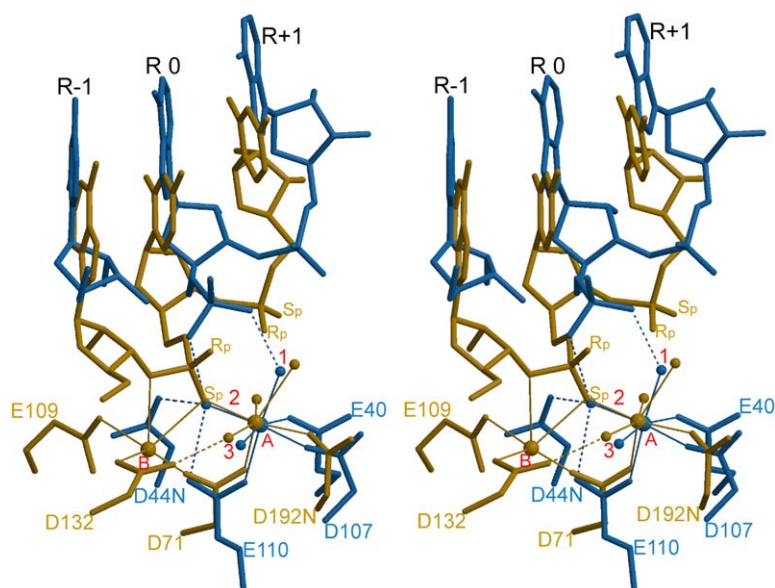


**Figure 7. Cleavage-Site Structure of RNase III and RNase H**

Stereoview showing the superposition of the cleavage site in Aa-D44N•RNA 6 (in blue) and in RNase H•RNA/DNA (in orange; Nowotny et al., 2005). Both amino acid and nucleotide residues are shown as stick models. Metal ions and water molecules are shown as spheres. The coordination bonds of  $Mg^{2+}$  are shown as solid lines and hydrogen bonds as dashed lines.

chemistry. The available structural and biochemical data suggest the requirement of a second divalent cation in the hydrolysis of each RNA strand by RNase III.

## EXPERIMENTAL PROCEDURES

### Construction of the Aa-RNase III (D44N) Expression Vector

The plasmid expression vector that was used to produce the Aa-D44N mutant was constructed by overlap extension PCR (Ho et al., 1989) and Gateway recombinational cloning (Invitrogen, Carlsbad, CA). A previously described Gateway entry clone of the open reading frame encoding full-length, wild-type Aa-RNase III was used as the template for PCR (Blaszczuk et al., 2004). Four oligodeoxyribonucleotides were used as PCR primers: (A) 5'-GGGGACAAGTTTGTACAAAAAAGCAGGCTTTAAG AAGGAGATATACATATGAAAATGTTGGAGCAACTG-3', (B) 5'-GGGG ACCACTTTGTACAAGAAAGCTGGGTTATTATTCTGATTCCTCCAGTAAT TT-3', (C) 5'-CACGAGGGCATTGCCGAGGAAGCT-3', and (D) 5'-GAGTT CCTCGGCAATGCCCTCGTG-3'. First, two separate PCRs were performed using primers A and C and primers B and D, respectively. The resulting PCR amplicons were combined and used as the template for another PCR with primers A and B. The final PCR amplicon was recombined into the entry vector pDONR201 to yield pBA1681, and then the nucleotide sequence of the entire ORF was confirmed. The ORF encoding the D44N mutant was then recombined into pDEST-42 (Invitrogen, Carlsbad, CA), a derivative of pET11 (Novagen, Madison, WI) to create the expression vector pBA1682.

### Protein Expression and Purification

The full-length Aa-D44N was overproduced in *E. coli* BL21(DE3) Codon-Plus-RIL cells (Stratagene, La Jolla, CA) and purified as described for the Aa-E110Q mutant (Gan et al., 2005). The final product, in 25 mM Tris (pH 7.2) 300 mM NaCl buffer, was concentrated to 16.8 mg/ml (determined spectrophotometrically using a molar extinction coefficient of 24,180  $M^{-1}cm^{-1}$ ). Aliquots were flash frozen in liquid nitrogen and stored at  $-80^{\circ}C$  until use. The Aa-D44N mutant was judged to be >95% pure by SDS-PAGE. The molecular weight was confirmed by electrospray mass spectrometry.

### RNA 5

Substrate RNA 5 (30-mer, 5'-AUAAAGGUCAUUCGCAAGAGUGGCCU UUAU-3') was purchased from Dharmacon RNA Technologies (Chicago)

and dissolved at 2.0 mM concentration in 25 mM Tris-HCl (pH 7.2) buffer containing 0.1 M NaCl.

### Crystallization and X-Ray Diffraction Data Collection

Prior to crystallization, the protein solution consisting of 9.3 mg/ml Aa-D44N, 0.8 mM RNA 5, 40 mM  $MgCl_2$ , and 280 mM NaCl in 25 mM Tris-HCl (pH 7.2) was incubated at  $75^{\circ}C$  for 30 min and then cooled down slowly to room temperature.

The crystallization screening was carried out with the sitting-drop vapor diffusion method at  $19^{\circ}C \pm 1^{\circ}C$ . Block-shaped single crystals (space group  $P2_1$ ; unit cell dimensions  $a = 63.8$ ,  $b = 51.0$ ,  $c = 113.8$  Å, and  $\beta = 104.5^{\circ}$ ) grew 3 months later from the drop containing 0.4  $\mu$ l protein solution and 0.2  $\mu$ l reservoir solution (0.2 M ammonium sulfate, 25% w/v PEG 3350 in 0.1 M HEPES [pH 7.5]) and reached the dimensions of  $0.10 \times 0.10 \times 0.02$  mm after 1 more month. The X-ray diffraction data were collected at the Southeast Regional Collaborative Access Team (SER-CAT) insertion device beamline 22 (22-ID) equipped with a Bruker Protom-300 CCD detector at the Advanced Photon Source, Argonne National Laboratory. Data processing was carried out with the HKL2000 program suite (Otwinowski and Minor, 1997). The completeness, redundancy,  $R_{merge}$  (defined as  $\Sigma|I - \langle I \rangle|/\Sigma I$ ), where  $I$  is the observed intensity), and  $I/\sigma(I)$  values for the entire data set (30.0–2.05 Å) are 90.6%, 2.5, 0.061, and 13.3, respectively, and the four values for the highest resolution shell (2.12–2.05 Å) are 55.2%, 1.6, 0.411, and 1.6, respectively.

### Structure Solution and Refinement

The structure of Aa-D44N•RNA 6 was solved with the molecular replacement program PHASER (McCoy et al., 2005; Reed, 2000; Storoni et al., 2004). Four structures, including Aa-E110K•RNA 1 (Blaszczuk et al., 2004), Aa-E110Q•RNA 2, Aa-RNase III•RNA 3 and Aa-RNase III•RNA 4 (Gan et al., 2005), were used to derive the search model ensembles for the endoND and the dsRBD. The MR solution, containing two endoNDs and two dsRBDs, was subjected to rigid-body refinement, energy minimization, and grouped B factor refinement followed by a difference Fourier synthesis, which revealed the position of RNA 6.

The structure was refined with the program CNS (Brünger et al., 1998) on a Silicon Graphics Fuel workstation. A total of 1932 (5%) reflections were randomly selected for crossvalidation ( $R_{free}$ ). Bulk solvent correction was employed. During the refinement, the  $2F_o - F_o$  and  $F_o - F_c$  electron-density maps were regularly calculated and examined. Solvent

molecules, as peaks  $\geq 3\sigma$  on the  $F_o - F_c$  map with reasonable hydrogen bond network, were included as water oxygen atoms at the later stage of the refinement. Upon completion, the entire structure was verified with the composite annealed omit map (Brünger et al., 1998). The final structure (crystallographic  $R = 0.206$ ,  $R_{free} = 0.257$ ) was assessed with PROCHECK (Laskowski et al., 1993), and 92.1% of the  $\phi/\psi$  values were found in the most favored regions on the Ramachandran plot. The rmsds for bond lengths and angle distances are 0.005 and 1.1 Å, respectively, and the estimated coordinate error is 0.27 Å. All graphics work was carried out using O (Jones et al., 1991). Illustrations were prepared with program packages MOLSCRIPT (Kraulis, 1991), BOBSCRIPT (Esnouf, 1997), RASTER3D (Merritt and Bacon, 1997), and GRASP (Nicholls et al., 1991).

## ACKNOWLEDGMENTS

We thank Mi Li and Gary Shaw for assistance during X-ray diffraction data acquisition, Marcin Nowotny and Wei Yang for access to their RNase H structures before publication, and Alexander Wlodawer and Allen Nicholson for insightful discussions and critical reading of the manuscript. Electrospray mass spectrometry experiments were conducted on the LC/ESMS instrument maintained by the Biophysics Resource in the Structural Biophysics Laboratory, National Cancer Institute. X-ray diffraction data were collected at the SER-CAT 22-ID beamline of the APS, Argonne National Laboratory. Supporting institutions may be found at [www.ser-cat.org/members.html](http://www.ser-cat.org/members.html). This research was supported by the Intramural Research Program of the NIH, National Cancer Institute, Center for Cancer Research.

Received: August 17, 2005

Revised: October 5, 2005

Accepted: November 10, 2005

Published: January 26, 2006

## REFERENCES

- Akey, D.L., and Berger, J.M. (2005). Structure of the nuclease domain of ribonuclease III from *M. tuberculosis* at 2.1 Å. *Protein Sci.* *14*, 2744–2750.
- Bernstein, E., Caudy, A.A., Hammond, S.M., and Hannon, G.J. (2001). Role for a bidentate ribonuclease in the initiation step of RNA interference. *Nature* *409*, 363–366.
- Blaszczyk, J., Tropea, J.E., Bubunenko, M., Routzahn, K.M., Waugh, D.S., Court, D.L., and Ji, X. (2001). Crystallographic and modeling studies of RNase III suggest a mechanism for double-stranded RNA cleavage. *Structure* *9*, 1225–1236.
- Blaszczyk, J., Gan, J., Tropea, J.E., Court, D.L., Waugh, D.S., and Ji, X. (2004). Noncatalytic assembly of ribonuclease III with double-stranded RNA. *Structure* *12*, 457–466.
- Brünger, A.T., Adams, P.D., Clore, G.M., DeLano, W.L., Gros, P., Grosse-Kunstleve, R.W., Jiang, J.S., Kuszewski, J., Nilges, M., Pannu, N.S., et al. (1998). Crystallography & NMR system: A new software suite for macromolecular structure determination. *Acta Crystallogr. D* *54*, 905–921.
- Calin-Jageman, I., and Nicholson, A.W. (2003). RNA structure-dependent uncoupling of substrate recognition and cleavage by *Escherichia coli* ribonuclease III. *Nucleic Acids Res.* *31*, 2381–2392.
- Campbell, F.E., Jr., Cassano, A.G., Anderson, V.E., and Harris, M.E. (2002). Pre-steady-state and stopped-flow fluorescence analysis of *Escherichia coli* ribonuclease III: insights into mechanism and conformational changes associated with binding and catalysis. *J. Mol. Biol.* *317*, 21–40.
- Carthew, R.W. (2001). Gene silencing by double-stranded RNA. *Curr. Opin. Cell Biol.* *13*, 244–248.
- Chang, K.Y., and Ramos, A. (2005). The double-stranded RNA-binding motif, a versatile macromolecular docking platform. *FEBS J.* *272*, 2109–2117.
- Conrad, C., and Rauhut, R. (2002). Ribonuclease III: new sense from nuisance. *Int. J. Biochem. Cell Biol.* *34*, 116–129.
- Conrad, C., Evgueniva-Hackenberg, E., and Klug, G. (2001). Both N-terminal catalytic and C-terminal RNA binding domain contribute to substrate specificity and cleavage site selection of RNase III. *FEBS Lett.* *509*, 53–58.
- Court, D. (1993). RNA processing and degradation by RNase III. In *Control of Messenger RNA Stability*, J.G. Belasco and G. Braverman, eds. (New York, NY: Academic Press), pp. 71–116.
- Dasgupta, S., Fernandez, L., Kameyama, L., Inada, T., Nakamura, Y., Pappas, A., and Court, D.L. (1998). Genetic uncoupling of the dsRNA-binding and RNA cleavage activities of the *Escherichia coli* endoribonuclease RNase III - the effect of dsRNA binding on gene expression. *Mol. Microbiol.* *28*, 629–640.
- Davies, D.R., Goryshin, I.Y., Reznikoff, W.S., and Rayment, I. (2000). Three-dimensional structure of the Tn5 synaptic complex transposition intermediate. *Science* *289*, 77–85.
- Dunn, J.J. (1982). Ribonuclease III. In *The Enzymes*, P. Boyer, ed. (New York, NY: Academic Press), pp. 485–499.
- Esnouf, R.M. (1997). An extensively modified version of MolScript that includes greatly enhanced coloring capabilities. *J. Mol. Graph. Model.* *15*, 132–134.
- Filippov, V., Solovyev, V., Filippova, M., and Gill, S.S. (2000). A novel type of RNase III family proteins in eukaryotes. *Gene* *245*, 213–221.
- Gan, J., Tropea, J.E., Austin, B.P., Court, D.L., Waugh, D.S., and Ji, X. (2005). Intermediate states of ribonuclease III in complex with double-stranded RNA. *Structure* *13*, 1435–1442.
- Guameros, G. (1988). Retroregulation of bacteriophage lambda int gene expression. *Curr. Top. Microbiol. Immunol.* *136*, 1–19.
- Ho, S.N., Hunt, H.D., Horton, R.M., Pullen, J.K., and Pease, L.R. (1989). Site-directed mutagenesis by overlap extension using the polymerase chain reaction. *Gene* *77*, 51–59.
- Inada, T., and Nakamura, Y. (1995). Lethal double-stranded RNA processing activity of ribonuclease III in the absence of suhB protein of *Escherichia coli*. *Biochimie* *77*, 294–302.
- Inada, T., Kawakami, K., Chen, S.M., Takiff, H.E., Court, D.L., and Nakamura, Y. (1989). Temperature-sensitive lethal mutant of ERA, a G protein in *Escherichia coli*. *J. Bacteriol.* *171*, 5017–5024.
- Jones, T.A., Zou, J.Y., Cowan, S.W., and Kjeldgaard. (1991). Improved methods for building protein models in electron density maps and the location of errors in these models. *Acta Crystallogr. A* *47*, 110–119.
- Krainer, A. (1997). *Eukaryotic mRNA Processing* (New York, NY: IRL Press).
- Kraulis, P.J. (1991). MOLSCRIPT: a program to produce both detailed and schematic plots of protein structures. *J. Appl. Crystallogr.* *24*, 946–950.
- Lamontagne, B., Larose, S., Boulanger, J., and Elela, S.A. (2001). The RNase III family: a conserved structure and expanding functions in eukaryotic dsRNA metabolism. *Curr. Issues Mol. Biol.* *3*, 71–78.
- Lamontagne, B., Ghazal, G., Lebars, I., Yoshizawa, S., Fourmy, D., and Elela, S.A. (2003). Sequence dependence of substrate recognition and cleavage by yeast RNase III. *J. Mol. Biol.* *327*, 985–1000.
- Laskowski, R.A., MacArthur, M.W., Moss, D.S., and Thornton, J.M. (1993). PROCHECK: a program to check stereochemical quality of protein structures. *J. Appl. Crystallogr.* *26*, 283–291.
- Lee, Y.S., Nakahara, K., Pham, J.W., Kim, K., He, Z., Sontheimer, E.J., and Carthew, R.W. (2004). Distinct roles for *Drosophila* Dicer-1 and Dicer-2 in the siRNA/miRNA silencing pathways. *Cell* *117*, 69–81.

- Li, H., and Nicholson, A.W. (1996). Defining the enzyme binding domain of a ribonuclease III processing signal. Ethylation interference and hydroxyl radical footprinting using catalytically inactive RNase III mutants. *EMBO J.* *15*, 1421–1433.
- McCoy, A.J., Grosse-Kunstleve, R.W., Storoni, L.C., and Read, R.J. (2005). Likelihood-enhanced fast translation functions. *Acta Crystallogr. D Biol. Crystallogr.* *61*, 458–464.
- Merritt, E.A., and Bacon, D.J. (1997). Raster3D: photorealistic molecular graphics. *Methods Enzymol.* *277*, 505–524.
- Nicholls, A., Sharp, K.A., and Honig, B. (1991). Protein folding and association: insights from the interfacial and thermodynamic properties of hydrocarbons. *Proteins* *11*, 281–296.
- Nicholson, A.W. (1996). Structure, reactivity, and biology of double-stranded RNA. *Prog. Nucleic Acid Res. Mol. Biol.* *52*, 1–65.
- Nicholson, A.W. (1999). Function, mechanism and regulation of bacterial ribonucleases. *FEMS Microbiol. Rev.* *23*, 371–390.
- Nowotny, M., Gaidamakov, S.A., Crouch, R.J., and Yang, W. (2005). Crystal structures of RNase H bound to an RNA/DNA hybrid: substrate specificity and metal-dependent catalysis. *Cell* *121*, 1005–1016.
- Oppenheim, A.B., Kornitzer, D., Altuvia, S., and Court, D.L. (1993). Post-transcriptional control of the lysogenic pathway in bacteriophage lambda. *Prog. Nucleic Acid Res. Mol. Biol.* *46*, 37–49.
- Otwinowski, Z., and Minor, W. (1997). Processing of X-ray diffraction data collected in oscillation mode. *Methods Enzymol.* *276*, 307–326.
- Reed, R.J. (2000). Pushing the boundaries of molecular replacement with maximum likelihood. *Acta Crystallogr. D Biol. Crystallogr.* *D57*, 1373–1382.
- Robertson, H.D. (1982). *Escherichia coli* ribonuclease III cleavage sites. *Cell* *30*, 669–672.
- Robertson, H.D., and Dunn, J.J. (1975). Ribonucleic acid processing activity of *Escherichia coli* ribonuclease III. *J. Biol. Chem.* *250*, 3050–3056.
- Robertson, H.D., Webster, R.E., and Zinder, N.D. (1968). Purification and properties of ribonuclease III from *Escherichia coli*. *J. Biol. Chem.* *243*, 82–91.
- Ryter, J.M., and Schultz, S.C. (1998). Molecular basis of double-stranded RNA-protein interactions: structure of a dsRNA-binding domain complexed with dsRNA. *EMBO J.* *17*, 7505–7513.
- Steiniger-White, M., Rayment, I., and Reznikoff, W.S. (2004). Structure/function insights into Tn5 transposition. *Curr. Opin. Struct. Biol.* *14*, 50–57.
- Storoni, L.C., McCoy, A.J., and Read, R.J. (2004). Likelihood-enhanced fast rotation functions. *Acta Crystallogr. D Biol. Crystallogr.* *60*, 432–438.
- Sun, W., and Nicholson, A.W. (2001). Mechanism of action of *Escherichia coli* ribonuclease III. Stringent chemical requirement for the glutamic acid 117 side chain and Mn(2+) rescue of the Glu117Asp mutant. *Biochemistry* *40*, 5102–5110.
- Sun, W., Jun, E., and Nicholson, A.W. (2001). Intrinsic double-stranded-RNA processing activity of *Escherichia coli* ribonuclease III lacking the dsRNA-binding domain. *Biochemistry* *40*, 14976–14984.
- Sun, W., Li, G., and Nicholson, A.W. (2004). Mutational analysis of the nuclease domain of *Escherichia coli* ribonuclease III. Identification of conserved acidic residues that are important for catalytic function in vitro. *Biochemistry* *43*, 13054–13062.
- Sun, W., Pertz, A., and Nicholson, A.W. (2005). Catalytic mechanism of *Escherichia coli* ribonuclease III: kinetic and inhibitor evidence for the involvement of two magnesium ions in RNA phosphodiester hydrolysis. *Nucleic Acids Res.* *33*, 807–815.
- Tian, B., Bevilacqua, P.C., Diegelman-Parente, A., and Mathews, M.B. (2004). The double-stranded-RNA-binding motif: interference and much more. *Nat. Rev. Mol. Cell Biol.* *5*, 1013–1023.
- Wu, H., Xu, H., Miraglia, L.J., and Crooke, S.T. (2000). Human RNase III is a 160-kDa protein involved in preribosomal RNA processing. *J. Biol. Chem.* *275*, 36957–36965.
- Yang, D., Buchholz, F., Huang, Z., Goga, A., Chen, C.Y., Brodsky, F.M., and Bishop, J.M. (2002). Short RNA duplexes produced by hydrolysis with *Escherichia coli* RNase III mediate effective RNA interference in mammalian cells. *Proc. Natl. Acad. Sci. USA* *99*, 9942–9947.
- Zhang, H., Kolb, F.A., Jaskiewicz, L., Westhof, E., and Filipowicz, W. (2004). Single processing center models for human Dicer and bacterial RNase III. *Cell* *118*, 57–68.
- Zhang, K., and Nicholson, A.W. (1997). Regulation of ribonuclease III processing by double-helical sequence antideterminants. *Proc. Natl. Acad. Sci. USA* *94*, 13437–13441.

#### Accession Numbers

The coordinates and structure factors reported herein have been deposited with the Protein Data Bank with the ID code [2EZ6](#).